BILINGUAL PUBLISHING GROUP

Journal of Environmental & Earth Sciences

https://journals.bilpubgroup.com/index.php/jees

ARTICLE

The Optimization of High-Temperature Dust Capture System in the Blast Furnace Tapping Field

Jianheng Zhuang [1,2] , ***Hui Wang*** [1,3,4*] , ***Yuan Dong*** [1,3] , ***Wen Li*** [1,3]

[1] *Central Research Institute of Building and Construction CO., Ltd., MCC Group, Beijing 100088, China*

[2] *Zhanjiang Environmental Protection Operation Management Co., Ltd., MCC Group, Zhanjiang 524000, China*

[3] *State Key Laboratory of Iron and Steel Industry Environmental Protection, Beijing 102600, China*

[4] *Energy Saving and Environmental Protection Co., Ltd., MCC Group, Beijing 100088, China*

ABSTRACT

During the tapping process of a blast furnace, a large amount of high-temperature dust is generated. Relying solely on dust removal systems to control the spread of dust within the workshop will generate huge energy consumption. Optimizing the high-temperature dust capture system is crucial for improving the working environment, reducing air pollution, and achieving energy savings and emission reductions. Considering the structural layout of workshops and the tapping characteristics of small and medium-sized blast furnaces in China, this study optimized the design of the particulate capture system by incorporating local dust hoods through numerical simulation, while also taking into account the local capture of particles at the hot metal ladle. The research found that to prevent dust escape, adding a small dust hood above the tapping hole and a side suction hood with a capacity of 100,000 m^3/h near the tap hole allowed all particles to be directly captured, reducing both their residence time and travel distance. Additionally, the height of thermal stratification within the workshop decreased, and the area of high-temperature zones was reduced. After adding a side suction hood in the hot metal ladle area, the temperature under the hood improved significantly, with the air temperature around the ladle dropping to approximately 40 ℃. When the side suction hood's airflow exceeded 100,000 m^3/h, the capture efficiency reached 99.2%.

*CORRESPONDING AUTHOR:

Hui Wang, Central Research Institute of Building and Construction CO., Ltd., MCC Group, Beijing 100088, China; State Key Laboratory of Iron and Steel Industry Environmental Protection, Beijing 102600, China; Energy Saving and Environmental Protection Co., Ltd., MCC Group, Beijing 100088, China; Email: wanghui@cribc.com

ARTICLE INFO

Received: 4 November 2025 | Revised: 13 December 2025 | Accepted: 26 December 2025 | Published Online: 31 December 2025

DOI: https://doi.org/10.30564/jees.v7i12.12852

CITATION

Zhuang, J., Wang, H., Dong, Y., et al., 2025. The Optimization of High-Temperature Dust Capture System in the Blast Furnace Tapping Field. Journal of Environmental & Earth Sciences. 7(12):60–72. DOI: https://doi.org/10.30564/jees.v7i12.12852

However, when the observation hole of the top suction hood above the ladle was opened, the temperature inside the hood decreased by 10 °C, and approximately 11.9% of the particles escaped through the observation hole into the workshop.
Keywords: Iron Tapping Area; High-Temperature Dust; Capture Optimization; Hot Metal Ladle; Numerical Simulation

1. Introduction

China ranks first globally in steel production, and the steel industry is a major polluter, with pollutant emissions ranking second among industrial atmospheric emissions. During the tapping process of blast furnaces in steel plants, tapping fields generate massive amounts of dust. The particulate matter generation coefficient for steelmaking pig iron in the blast furnace cast house is 8.06 kg per ton of product[1]. Additionally, this dust features high temperature and small particle size, which severely endangers workers' health[2,3]. For most small and medium-sized steel plants, their workshops are mostly open or semi-enclosed, leading to unorganized emission of most dust into the environment and causing severe particulate pollution[4].

The emission of high-temperature dust from tapping fields is not only characterized by strong intermittency and long duration but also poses multiple pollution challenges due to its wide particle size distribution and extensive diffusion range[5]. Compared with general ventilation, local ventilation can precisely control the airflow around pollution sources and efficiently collect pollutants and reduce ventilation energy consumption[6–9]. Scholars have conducted numerous studies on improving the capture efficiency and optimizing the performance of local exhaust hoods. Wang and Zhang 1[10] performed theoretical calculations for the upper-suction dust hood to address flue gas dust removal at the tapping hole of blast furnace tapping fields, and derived the theoretical dimensions of the exhaust hood and its optimal position at the pollution source, as well as the optimal air extraction volume for flue gas capture. Research efforts have focused on both structural improvements to hoods[11] and on flow control modifications, such as using flanges[12] or partition plates[13] to optimize the velocity distribution at the hood opening. Zhang et al.[14] used CFD simulation to study the impact of exhaust outlet position and height on the flow field under given conditions of air supply outlet location, number of air supply outlets, and number of exhaust outlets, analyzing the flow characteristics inside the air collection hoods under different geometric flow field boundaries. Guo and Bao[15] first used CFD software to simulate the airflow field to determine the air volumes of the exhaust system, then adopted laboratory simulation tests to measure the capture efficiency at control points. They studied the influence of parameters such as the height of the exhaust hood, baffle width, and exhaust air volume on pollutant control effects, concluding that the capture efficiency and control distance present a polynomial relationship. Based on the analysis of specific engineering cases, Huang et al. [16][7] proposed schemes to optimize and improve the capture efficiency of local exhaust hoods. The results showed that the capture efficiency of local exhaust hoods is inversely proportional to the distance from the pollution source and is directly proportional to the initial emission velocity of pollutants. Under the condition of limited buoyant jet space, Liu[16] proposed an optimization method for exhaust hoods, which involves arranging inclined baffles and vertical side plates on the opposite side of the exhaust hood to enhance pollutant capture effects. They revealed the influence of hood opening wind speed and the distance between the source and the hood on capture efficiency; at a specific distance, increasing the average wind speed at the hood opening can further improve capture efficiency. Song et al.[17] conducted a numerical simulation of airflow organization for semi-closed dust hoods in typical foundries, controlling dust escape from upper openings through a reasonable arrangement of suction ports. Zhang et al.[18] determined the optimal layout form, position, height, air volume, and other parameters of exhaust hoods through numerical simulation to address airflow control and waste heat treatment above high-temperature heat sources during industrial production. Ren and Wang[19] applied the discrete phase model to numerically simulate the flow field inside local exhaust hoods under two-phase flow conditions, improving capture efficiency by adjusting air volume, exhaust hood height, wind deflectors, and other means, while avoiding blind increases in fan energy consumption. Wang et al.[20] studied the flow field characteristics inside the swing nozzle and semi-closed hood of hot metal ladles through

numerical simulation, improving the capture efficiency of exhaust hoods.

Dust in blast furnace tapping fields is mainly generated at the tapping hole, main trough, skimmer, iron trough, hot metal ladle, and during the operation of opening and plugging the tapping hole [21–25]. The original design method of the tapping hole dust hood has certain limitations, and problems such as low capture efficiency and high energy consumption often occur in practical applications [26]. By comparing the flow fields, temperature fields, and particle diffusion and capture laws under different ventilation and dust removal methods, Wang et al. [5] found that adding a dust hood at the tapping hole for typical confined space thermal plumes improved the temperature field of the tapping field and enhanced particle capture efficiency. They also found that the high-speed ascending airflow in the gap between the dust hood and the blast furnace caused particle escape in front of the main trough, and the particle capture effect in the hot metal ladle area was poor due to the large distance from the dust hood. This study optimizes the particle capture system after adding dust hoods, while considering the local capture of particles at the hot metal ladle, to improve the overall particle capture rate of the tapping field and provide a reference for the setting of dust hoods and the improvement of workshop forms.

2. Numerical Simulation

2.1. Physical Model

The research object is a 1080 m³ blast furnace of an iron and steel enterprise with an annual output of 13 million tons in Shandong Province, which is simplified as a cylinder. The actual dimensions of the workshop are 50 m × 24 m × 12.4 m, the size of the air inlet window is 24 m × 2 m, and the size of the top skylight is 18 m × 4 m. The bottom of the dust hood is 4 m × 4 m, the top is 2 m × 2 m, and the height is 2 m. The bottom of the large dust hood (Hood 1) is 4 m above the ground, and its axis is 7 m away from the blast furnace axis. Due to the limitations of installation conditions in the workshop, the large dust hood at the tapping hole cannot be closely attached to the blast furnace. Therefore, an additional local small dust hood (Hood 2) is installed at the top in front of the blast furnace. To capture particles generated by dust sources behind the iron trough, a local side suction hood (Hood 3) is installed in front of the first hot metal ladle in the tapping field. The two small dust hoods have the same size: the bottom is 2 m × 2 m, the top is 1 m × 1 m, and the height is 1 m. The axis of the dust hood above the blast furnace is 5.3 m away from the blast furnace axis, and the dust hood in front of the iron trough is 1 m away from the first tapping hole. The positions of the dust hoods are shown in **Figure 1a**.

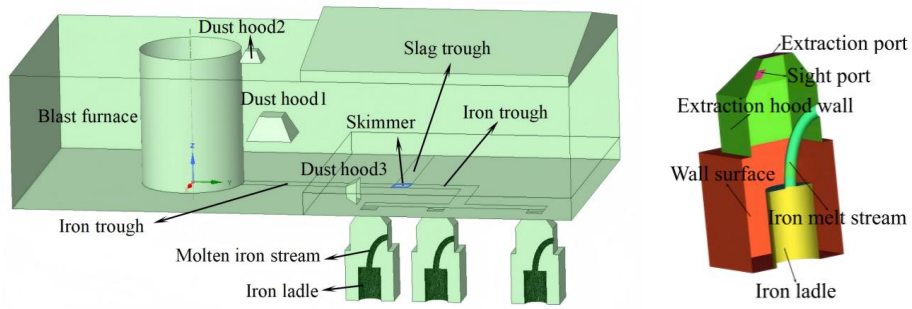

(**a**) (**b**)

Figure 1. Schematic Diagram of: (**a**) Tapping Field Space; (**b**) Local Hot Metal Ladle.

The molten iron flows out of the blast furnace, along the iron trough, and after skimming, flows into the three local hot metal ladles below. Since most small and medium-sized steel plants have installed closed dust hoods above the hot metal ladles on the tapping platform, the hot metal ladle area can be separated to study the particle emission and capture process. The schematic diagram of the local space of the hot metal ladle is shown in **Figure 1b**. The section plane is a symmetry plane. The height of the entire area is 8.2 m, the hot metal ladle is simplified as a cylinder with a diameter of 2 m and a height of 3 m, the diameter of the molten iron column is 0.5 m, and the size of the top suction port is 1.4 m × 1.4 m. The bottom size is 4.3 m × 6 m, and the size of the observation hole is 0.6 m × 0.6 m.

2.2. Numerical Calculation

2.2.1. Boundary Conditions and Mesh Generation

In the tapping field area, the lower windows are set as free air inlets, and the upper windows as free air outlets. The particles generated by the flowing molten iron in the tapping field mainly come from the oxidation reaction between molten iron and surrounding air, and their main component is iron oxide. The temperature of molten iron is as high as 1400℃, and intense natural convection occurs above it, forming a high-temperature plume. The flowing molten iron can be simplified as a high-temperature heat source surface, and particles are emitted and tracked using the Lagrangian method to obtain comprehensive information on their emission, diffusion, and capture processes. Other structures, such as the mud gun room in the tapping field, are ignored. In actual production, the main trough area is frequently operated by equipment such as mud guns, so no trough cover is usually installed. Although the iron trough is equipped with a cover, a large amount of dust still escapes from the connecting gaps, which can be simplified as several local dust sources. Therefore, six particle emission areas are set along the flow path of molten iron in this study, namely the front section of the main trough (tapping hole), the middle section of the main trough, the skimmer, and three dust emission points of the iron trough (as shown in **Figure 1**). To study the diffusion and capture laws of particles under different air volumes of the top suction hood, the air volumes of tsg_case2 and tsg_case3 are set to 100,000 m³/h and 150,000 m³/h, respectively, with other conditions the same as tsg_case1.

The mesh of the hot metal ladle area is divided into tetrahedral meshes with local refinement. The boundary conditions for the flow field, temperature field, and particle phase are set the same as those for the tapping field. **Table 1** shows the boundary conditions of the hot metal ladle simulation area. It is considered that more than 50% of the unorganized emissions from the iron casting field are iron oxide. Therefore, the particle parameters are taken as iron oxide parameters, with a density of 4580 kg/m^3, a diameter of 10 mm, a thermal conductivity of 0.55 w/m·K, and a specific heat capacity of 710 J/kg·K. Particles are emitted from the upper part of the hot metal ladle with a velocity of 2 m/s and a mass flow rate of 45.94 g/s.

Table 1. Boundary Conditions of Local Space of Hot Metal Ladle.

Surface	Boundary Condition		
	Tsg_case1	Tsg_case2	Tsg_case3
Observation Hole	Wall	Pressure-outlet, 0 Pa, 25 ℃	
Ventilation Port	Velocity outlet, 25 ℃, 100,000 m^3/h	Velocity outlet, 25 ℃, 100,000 m^3/h	Velocity outlet, 25 ℃, 150,000 m^3/h
Suction Hood Wall	30 ℃		
Molten Iron Column, Upper Part of Hot Metal Ladle	1400 ℃		
Free Boundary, Lower Part	Pressure-outlet, 0 Pa, 25 ℃		
Wall Surface	25 ℃		
Hot Metal Ladle	200 ℃		

2.2.2. Model Setup and Validation

FLUENT is used to calculate the two-phase flow field, temperature field, and particle trajectory in the tapping field. The simulation employed the realizable k-ε turbulence model with standard wall treatment, coupled with the discrete ordinates (DO) radiation model. For numerical solution, the SIMPLE algorithm was used for pressure-velocity coupling. Discretization was handled by the body force weighted scheme for pressure and the second-order upwind scheme for all other variables. Since the temperature range designed in this study is large, the airflow is subject to significant buoyancy caused by density differences. Therefore, the thermal effects option is enabled, and the full buoyancy effects option is selected. Due to the large temperature difference involved in the calculation, a linear piecewise calculation is performed for physical properties such as density, specific heat capacity, and viscosity. The capture efficiency of the dust hood for particles is calculated as the ratio of the number of particles captured by the dust hood to the total number of particles emitted from the emission points.

To verify mesh independence, meshes with different numbers and different wall refinement methods are divided. The natural ventilation volume of the workshop without a dust hood is used as the verification standard. The flow fields

are calculated for mesh numbers of 5.04 million, 9.36 million, and 27.40 million, respectively. When the number of grids exceeds 9.36 million, the rate of change in ventilation volume is less than 1%. Therefore, 9.36 million meshes are used for subsequent simulation calculations. Meanwhile, theoretical calculation verification is carried out in this study. The heat release Q = 561.40 kW and exhaust air temperature tp = 31 ℃ are obtained by measuring the high-temperature heat source surfaces and the blast furnace in the workshop. Taking calculated outdoor temperature of twf = 25 ℃ and air specific heat c = 1.007 kJ·℃/kg, mass flow rate G = 92.92 kg/s is calculated according to the formula Q = cG(tp-twf)/3600. This differs by only 0.6% from G = 93.46 kg/s calculated with 9.36 million meshes. Therefore, it is considered that the ventilation volume calculated with 9.36 million meshes is accurate and reliable.

3. Results and Discussion

3.1. Impact of Additional Local Dust Hoods on Exhaust Hood System Performance

3.1.1. Velocity and Temperature Distribution in the Tapping Field

Figure 2 shows the velocity distribution on the x = 0 plane after adding Hood 2 between the blast furnace and Hood 1. The simulation details of Hood 1 alone can be found in Wang et al.[5]. Due to the additional Hood 2 above the blast furnace, the suction force of the dust hood on the airflow in front of the blast furnace is enhanced, which is beneficial for particle capture. The upward airflow velocity under the dust hood increases. If particles generated at the main trough and tapping hole in front of Hood 1 escape from the gap between Hood 1 and the blast furnace, they can also be fully captured by Hood 2. The airflow in the upper front of the tapping field moves towards the roof vents, and there is no airflow moving from above the blast furnace to the roof vents.

It can be seen from **Figure 3** that obvious thermal stratification is formed near the blast furnace in the tapping field in the height direction. A typical thermal plume appears above the main trough, and all thermal plumes are discharged through the two dust hoods, which will greatly facilitate the capture of particles released above the molten iron.

In summary, after adding Hood 2 and Hood 3, the airflow circulation in front of the tapping field changes. The airflow at the roof dust removal vents mainly comes from the ascending airflow in front of and on both sides of the dust hood at a certain distance, rather than the ascending airflow in front of the blast furnace. All plumes generated by the main trough can be collected by the dust hoods, and no plumes escape from the dust hoods in front of the blast furnace, thus improving the capture efficiency of the dust removal system for high-temperature dust.

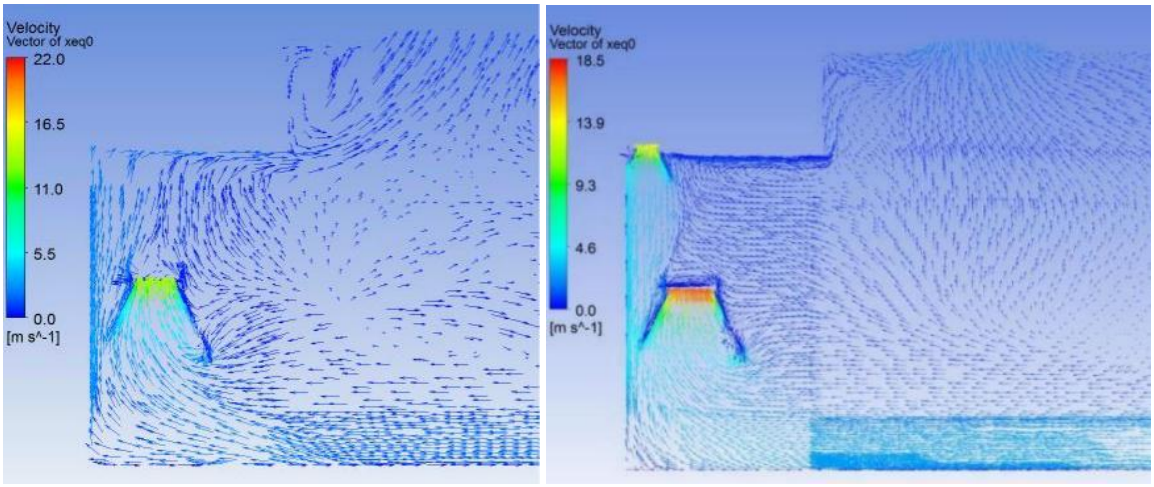

(**a**) Dust Hood 1 without Dust Hood 2 (Velocity Vector). (**b**) Dust Hood 1 with Dust Hood 2 (Velocity Vector).

Figure 2. Velocity Vector Diagrams of x = 0 m Plane with and without Dust Hood 2.

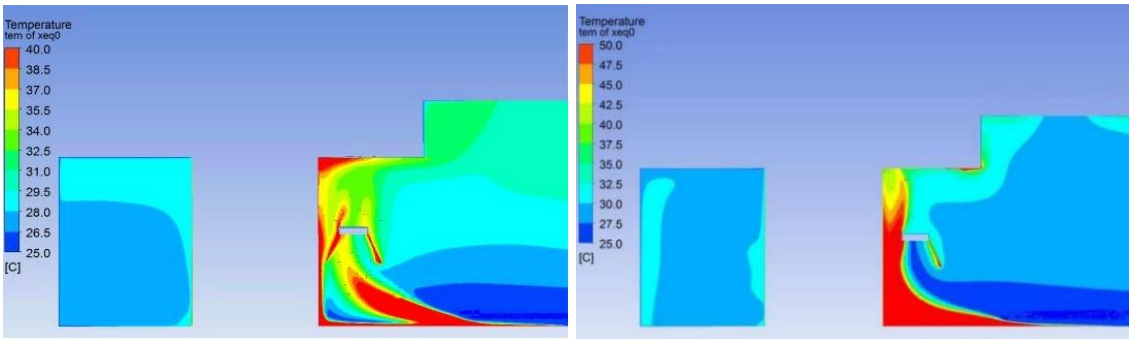

(**a**) Dust Hood 1 without Dust Hood 2 (Temperature). (**b**) Dust Hood 1 with Dust Hood 2 (Temperature).

Figure 3. Temperature Contour Maps of x = 0 m Plane.

3.1.2. Particle Emission and Capture Characteristics

After installing Hood 2 and Hood 3, the statistics of particle destinations at each dust generation point are shown in **Table 2**. All particles released from the front of the main trough, the middle of the main trough, the skimmer, dust source 1, and dust source 2 are captured by the dust hoods, with a capture efficiency of 100%.

Table 2. The statistics of particle destinations at each dust generation point.

	Front of Main Trough	Middle of Main Trough	Skimmer	Dust Source 1	Dust Source 2	Dust Source 3	Total
Tracked	1440	3300	1050	1050	750	205	7795
Escaped	0	0	0	0	0	0	0
Trapped	1440	3300	1050	1050	750	205	7795

Further analysis of the particle movement laws and capture characteristics at each dust generation point. **Figure 4** shows the trajectory diagrams of particles released from the front of the main trough, the middle of the main trough, the skimmer, dust source 1, and dust source 2 in case9. All particles generated by the dust sources on the center line of the tapping field are captured by Hood 1 and Hood 2 in front of the tapping hole, while particles generated by dust source 2 and dust source 3 behind the iron trough are directly captured by Hood 3. The residence time of particles is less than 10 s, and the workshop area they pass through is minimized. The improved dust removal system can achieve a clean workshop.

By adding a small dust hood above the tapping hole and a small side suction hood near the iron trough, with the air volume increased by 100,000 m³/h, all particles in the tapping field workshop are directly captured, with short residence time and travel distance, realizing a clean workshop. In addition, due to the increase in ventilation volume in the workshop, the height of thermal stratification in the workshop is reduced, and the area of high-temperature zones is decreased.

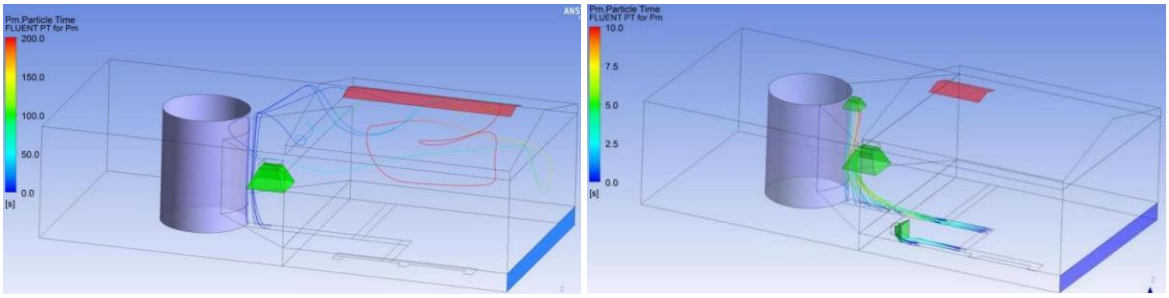

(**a**) Dust Hood 1. (**b**) Dust Hood 1–3.

Figure 4. Particle Trajectory Diagrams from Particle Emission Sources before and after Adding Dust Hoods.

3.2. Impact of Air Volume of Top Suction Hood in Hot Metal Ladle Area on Particle Emission and Capture

3.2.1. Flow Field and Temperature Field in Hot Metal Ladle Area

Figure 5 shows the axial velocity distribution curves on the center line under the top suction hood for tsg_case1, tsg_case2, and tsg_case3, with air volumes of 32.26 kg/s, 16.13 kg/s, and 48.39 kg/s, respectively. The axial velocity on the center line is the superposition of the ascending velocity of the thermal plume and the suction velocity of the top suction hood, which first increases and then decreases from bottom to top. It can be seen that the air volume has the most obvious effect on improving the axial velocity at a height of 7.3–8.2 m above the ground. Below 6.5 m, when the air volume exceeds 100,000 m³/h, the improvement of axial velocity is no longer obvious, and the axial velocity is above 10 m/s.

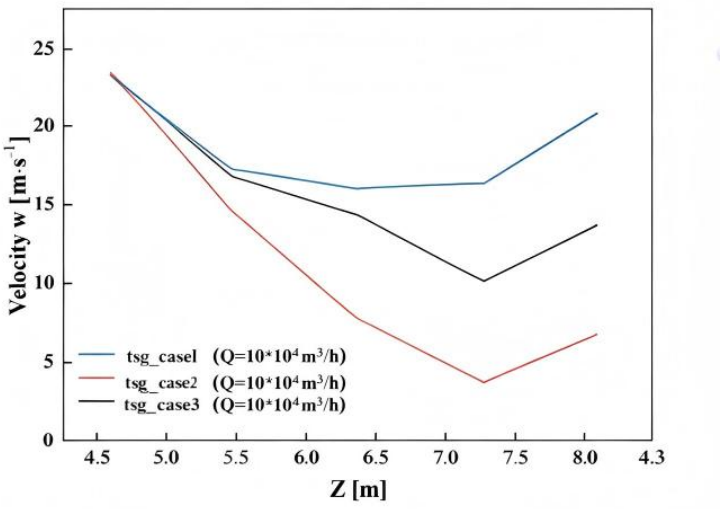

Figure 5. Axial Velocity Distribution on the Central Line under the Top Suction Hood of Hot Metal Ladle.

Figure 6 shows the velocity contour maps on the x = 0 plane for tsg_case1, tsg_case2, and tsg_case3. It can be seen that the velocity contour maps of the three cases show the same distribution law: a strong plume is generated above the molten iron column, and the larger the air volume, the larger the range of the plume. There is a large low-velocity zone in the middle of the left inlet, and a large-area recirculation zone at the left inlet. Meanwhile, under the top suction hood, when the air volume is 50,000 m³/h and 100,000 m³/h, there is also a downward recirculation zone. When the air volume reaches 150,000 m³/h, there is no recirculation zone under the top suction hood. If particles enter the recirculation zone, they may be carried to the left free outlet and discharged into the atmosphere.

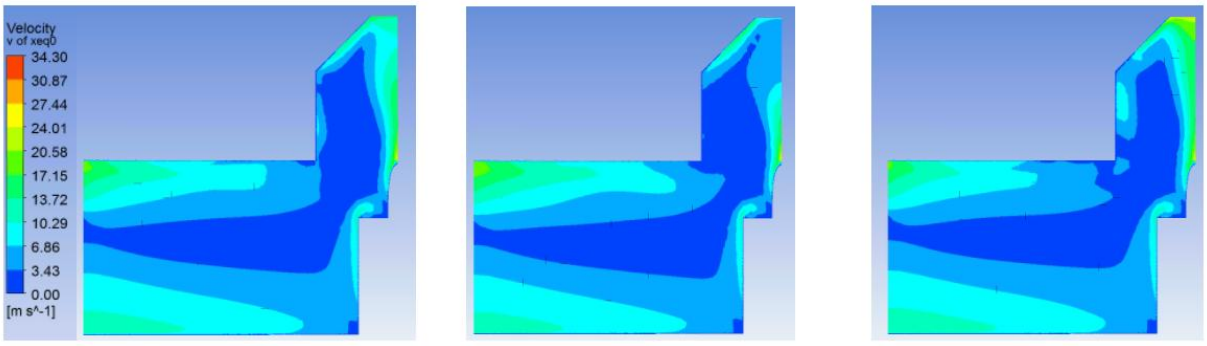

(**a**) (**b**) (**c**)

Figure 6. Velocity Contour Maps of x = 0 m Plane for: (**a**) tsg_case1; (**b**) tsg_case2; (**c**) tsg_case3.

Figure 7 shows the velocity contour maps on the y = 0 plane for tsg_case1, tsg_case2, and tsg_case3. It can be seen that a typical plume is formed above the molten iron column, and its velocity first increases and then decreases. The larger the air volume, the higher the height of the high-velocity zone of the plume. The air velocity on the side far from the molten iron column is much lower than the plume velocity. **Figure 8** shows the streamline diagrams starting from the free inlet for tsg_case1, tsg_case2, and tsg_case3. It can be seen that there is an obvious recirculation zone at the inlet. The airflow entering from the bottom rises after encountering the hot metal ladle and is discharged through the top suction port of the top suction hood. The larger the air volume at the suction port, the greater the depth of the recirculation zone in the y direction, and the shorter the residence time of the airflow discharged from the suction port.

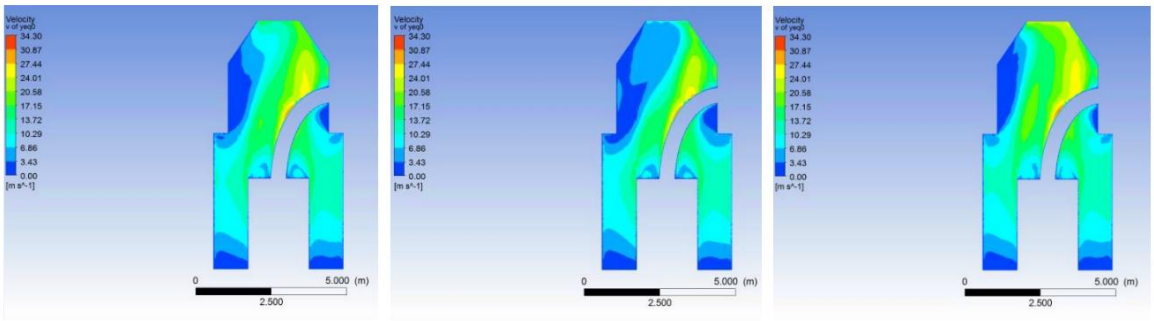

(**a**) (**b**) (**c**)

Figure 7. Velocity Contour Maps of y = 0m Plane for: (**a**) tsg_case1; (**b**) tsg_case2; (**c**) tsg_case3.

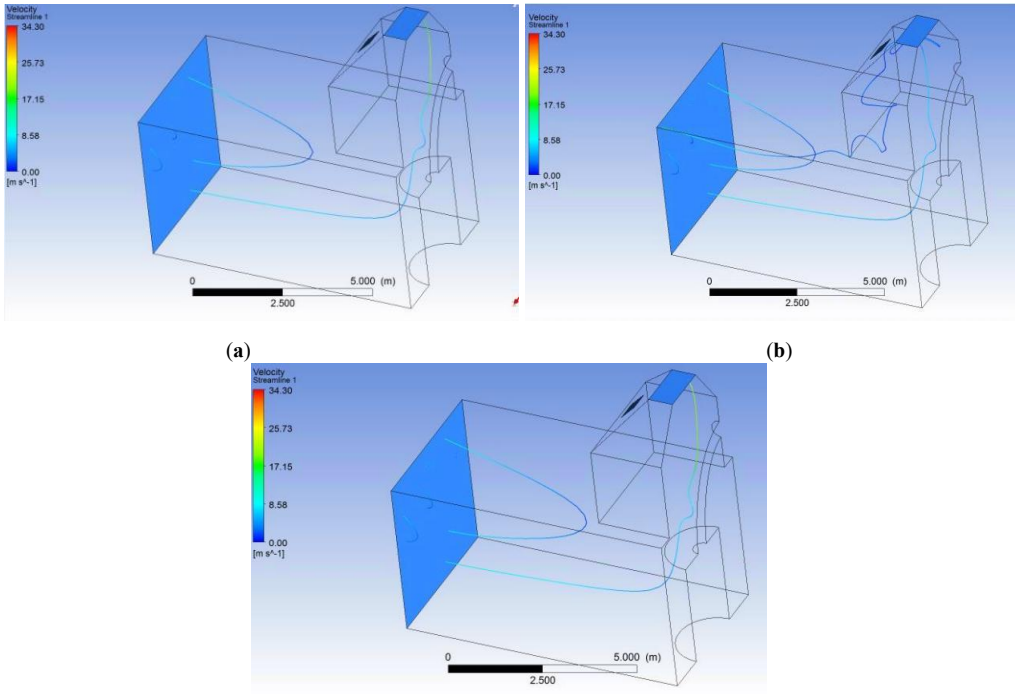

(**a**) (**b**)

(**c**)

Figure 8. Streamline Diagrams Starting from Free Inlet for: (**a**) tsg_case1; (**b**) tsg_case2; (**c**) tsg_case3.

Figure 9 shows the temperature contour maps on the x = 0 plane for tsg_case1, tsg_case2, and tsg_case3. It can be seen that thermal stratification is formed under the top suction hood, and the larger the air volume, the higher the temperature under it. When the air volume is 50,000 m^3/h, the temperature within 1.5 m from the top face is above 75 °C, which has a great impact on the service life of the dust hood. When the air volume is 100,000 m^3/h, the temperature

under the dust hood drops below 58 ℃.

In summary, a pronounced recirculation zone forms at the free inlet in the hot metal ladle area, where the temperature above the molten iron column exceeds 80 ℃. When the ventilation volume surpasses 100,000 m^3/h, the temperature beneath the dust hood is notably improved, stabilizing the ambient air temperature around the ladle at approximately 40 ℃. Under this airflow condition, the capture efficiency of the hood reaches 99.2%; thus, further increasing the air volume is deemed unnecessary.

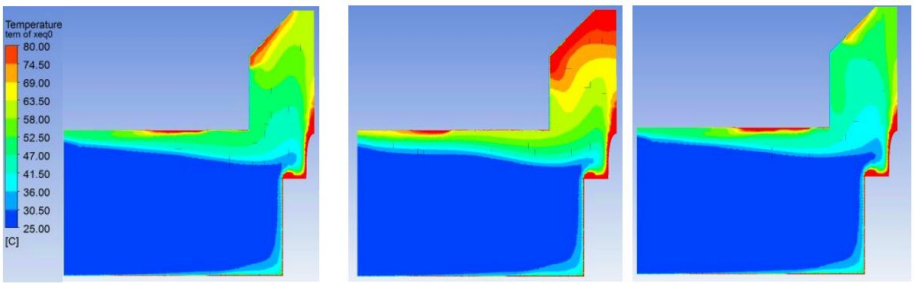

(**a**) (**b**) (**c**)

Figure 9. Temperature Contour Maps of x = 0 m Plane for: (**a**) tsg_case1; (**b**) tsg_case2; (**c**) tsg_case3.

3.2.2. Particle Emission and Diffusion Characteristics in Hot Metal Ladle Area

To compare the capture effects of dust hoods with different air volumes, the DPM model is used to track the trajectories of particles emitted from the upper surface of the hot metal ladle and count their final destinations. The results are shown in **Table 3**. The boundary conditions of DPM are: a trap for the suction port, escape for the free inlet, and reflect for other walls. The capture efficiencies (%) of the dust hoods under the three working conditions are calculated as 99.2%, 71.4%, and 100%, respectively. It can be seen that when the air volume of the dust hood exceeds 100,000 m^3/h, the capture efficiency has reached 99.2%, and further increasing the air volume is unnecessary.

Table 3. Statistics on the Number of Particle Destinations Released from the Hot Metal Ladle.

Boundary Conditions of DPM	tsg_case1	tsg_case2	tsg_case3
Tracked	126	126	126
Escaped	1	36	0
Trapped	125	90	126

Further analysis of the particle movement laws and capture characteristics at each dust generation point. **Figure 10** shows the trajectory diagrams of particles released from the upper surface of the hot metal ladle for tsg_case1, tsg_case2, and tsg_case3. It can be seen that when the air volume is 50,000 m^3/h, some particles are entrained into the vortex below the hot metal ladle and eventually discharged through the recirculation zone of the free inlet, and these particles have a long residence time in the hot metal ladle area. Most particles rise directly above the top suction hood with the thermal plume and are discharged through the suction port.

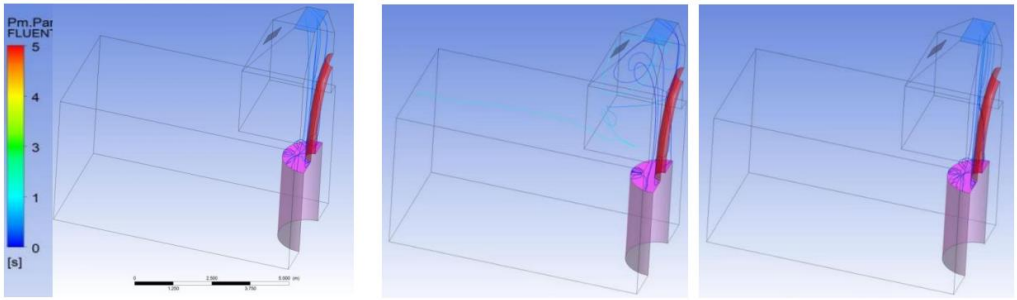

Figure 10. Velocity Contour Map of x = 0 Plane after Opening the Observation Hole.

3.3. Impact of Opening/Closing of Observation Hole in Hot Metal Ladle Area on Particle Emission and Diffusion

3.3.1. Flow Field and Temperature Field in Hot Metal Ladle Area

Figure 11 shows the velocity contour map on the x = 0 plane after opening the observation hole. Compared with tsg_case1, the maximum velocity at the observation hole after opening can reach 34 m/s. The simulated air mass flow rate of the observation hole is 9.51 kg/s, and the calculated average gas velocity is 22.75 m/s, which is higher than the average velocity of 14.17 m/s at the suction port of the dust hood. The vortex below the observation hole disappears.

Figure 12 shows the streamline diagram starting from the free inlet after opening the observation hole. Similar to tsg_case1, there is an obvious recirculation zone at the inlet. The airflow below the free inlet rises along the molten iron pipe, part of which is discharged by the top suction port of the top suction hood, and the other part is discharged through the observation hole. This part of the airflow may carry particles to escape from the top suction hood into the tapping field.

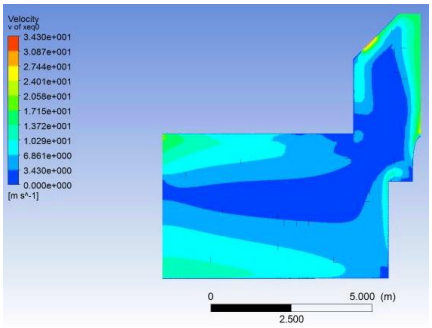

Figure 11. Velocity Contour Map of x = 0 Plane after Opening the Observation Hole.

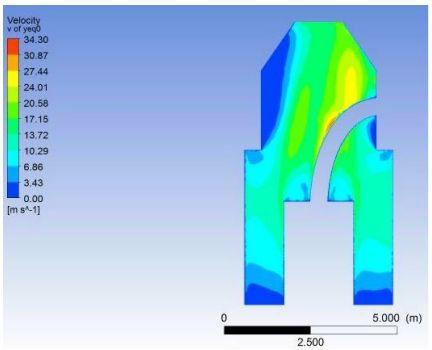

Figure 12. Velocity Contour Map of y = 0 Plane after Opening the Observation Hole.

Figure 13 shows the temperature contour map on the x = 0 m plane after opening the observation hole. It can be seen that after opening the observation hole, the temperature at the left top inside the top suction hood drops from the original 80 ℃ to 70 ℃. At the same time, the height of the thermal stratification increases accordingly.

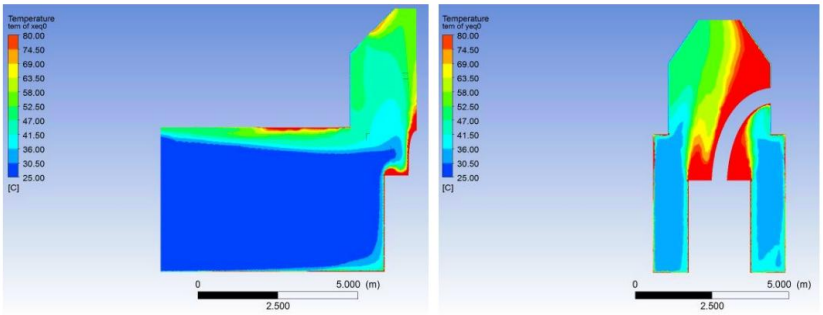

Figure 13. Temperature Contour Map of x = 0 m Plane for tsg_case4.

3.3.2. Particle Emission and Capture Characteristics in Hot Metal Ladle Area

The DPM model is used to track the trajectories of particles emitted from each dust generation point and count their final destinations. The results are shown in **Table 4**. The boundary conditions of DPM are: escape for the suction port and free inlet, trap for the observation hole, and reflect for other walls. The escape ratio (%) of the observation hole is defined as the ratio of trapped particles to the total tracked particles. The results are shown in **Table 4**. The capture efficiency of the top suction hood above the hot metal ladle is 11.9%; that is, after opening the observation hole, about 11.9% of the particles escape into the tapping field workshop through the observation hole.

Figure 14 shows the trajectory diagram of particles released from the upper surface of the hot metal ladle in tsg_case4. It can be seen that after particles are released from the upper surface of the hot metal ladle, most of them rise directly to the suction port with the airflow and are captured by the top suction hood, while a small number of particles enter the airflow near the observation hole and eventually escape through the observation hole. Therefore, when the observation hole on the top suction hood is opened, the velocity of the center line under the top suction hood increases to more than 14 m/s, and the ventilation volume of the observation hole can reach 59% of that of the suction port. The temperature inside the top suction hood decreases by about 10 ℃. After opening the observation hole, compared with the closed state, about 11.9% of the particles escaped into the tapping field workshop through the observation hole, causing significant pollution to the workshop.

Table 4. Statistics on the Number of Particle Destinations Released from the Upper Surface of Hot Metal Ladle in tsg_case4.

Tracked	Escaped	Trapped
126	111	15

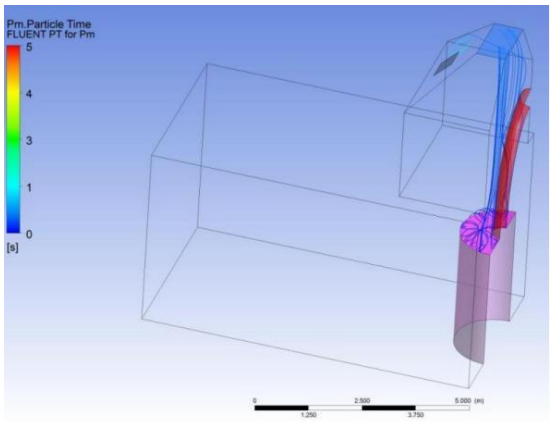

Figure 14. Particle Trajectory Diagram Released from the Upper Surface of Hot Metal Ladle for tsg_case4.

4. Conclusion

Adding a small dust hood above the tapping hole and a small side suction hood near the iron trough, with the air volume increased by 100,000 m³/h, can fully directly capture all particles in the tapping field workshop, with short residence time and travel distance, realizing a clean workshop. In addition, due to the increase in ventilation volume in the workshop, the height of thermal stratification in the workshop is reduced, and the area of high-temperature zones is decreased.

There is a large recirculation zone at the free inlet in the hot metal ladle area. The temperature above the molten iron column can reach more than 80 ℃. When the air volume exceeds 100,000 m³/h, the temperature under the dust hood can be significantly improved, and the ambient air temperature around the hot metal ladle is about 40 ℃. When the air volume of the dust hood exceeds 100,000 m³/h, the capture efficiency has reached 99.21%, and further increasing the air volume is unnecessary.

When the observation hole on the top suction hood is opened, the temperature above the inside of the top suction hood decreases by about 10 ℃. Compared with the closed

state of the observation hole, about 11.9% of the particles escape into the tapping field workshop through the observation hole after opening, causing significant pollution to the workshop.

Author Contributions

J.Z.: conceptualization, methodology, writing—original draft, supervision, project administration, funding acquisition; H.W.: software, data curation, formal analysis, writing—original draft; Y.D.: validation, formal analysis, writing—review and editing; W.L.: validation, writing—review and editing. All authors have read and agreed to the published version of the manuscript.

Funding

This work is supported by the State Key Laboratory Special Programs of China Minmetals Corporation (Grant No.2024GZGJ02).

Institutional Review Board Statement

Not applicable.

Informed Consent Statement

Not applicable.

Data Availability Statement

Data is not available due to privacy restrictions.

Conflicts of Interest

The authors declare no conflict of interest. The funders had no role in the design of the study; in the collection, analyses, or interpretation of data; in the writing of the manuscript; or in the decision to publish the results.

References

[1] Ministry of Ecology and Environment of the People's Republic of China (MEE), 2021. Manual of Pollutant Generation and Emission Coefficient for Emission Source Statistics Survey. MEE: Beijing, China. (in Chinese)

[2] Zhao, X., Yin, Y., 2024. Hazards of pollutants and ventilation control strategy in industrial workshops: Current state and future trend. Building and Environment. 251, 111229. DOI: https://doi.org/10.1016/j.buildenv.2024.111229

[3] Wang, H., Wang, T., Liu, L., et al., 2021. Numerical evaluation of the performances of the ventilation system in a blast furnace casthouse. Environmental Science and Pollution Research. 28(36), 50668–50682. DOI: https://doi.org/10.1007/s11356-021-14215-8

[4] Wang, H., Liu, L., Wang, T., et al., 2023. Influence of outdoor meteorological parameters on the indoor environment of blast furnace yard. Environmental Science and Pollution Research. 30(33), 80512–80529. DOI: https://doi.org/10.1007/s11356-023-28087-7

[5] Wang, T., Yang, J., Zhu, X., et al., 2021. Experimental Research on Dust Concentration Distribution Characteristics of Blast Furnace Cast House. IOP Conference Series: Earth and Environmental Science. 687(1), 012018. DOI: https://doi.org/10.1088/1755-1315/687/1/012018

[6] Zhang, J., Wang, J., Gao, J., et al., 2024. Exhaust hood performance and its improvement technologies in industrial buildings: A literature review. Building Simulation. 17(1), 23–40. DOI: https://doi.org/10.1007/s12273-023-1040-2

[7] Huang, Y., Lu, K., Guo, J., et al., 2020. Study on ventilation performance of lateral exhaust hood under the influence of two high-temperature buoyant jets. Building and Environment. 177, 106849. DOI: https://doi.org/10.1016/j.buildenv.2020.106849

[8] Fan, J.-N., Yang, Y., Wang, Y., et al., 2022. Emission and local ventilation control of droplets generated by condensation and bubble-bursting during pickling. Sustainable Cities and Society. 76, 103491. DOI: https://doi.org/10.1016/j.scs.2021.103491

[9] Cao, Z., Liu, Z., Zhang, C., et al., 2024. Performance analysis of a novel movable exhaust ventilation system for pollutant removal in industrial environments. Journal of Building Engineering. 97, 110569. DOI: https://doi.org/10.1016/j.jobe.2024.110569

[10] Wang, H., Zhang, P., 2021. Emission characteristics of PM, heavy metals, and dioxins in flue gases from sintering machines with wet and semi-dry flue gas desulfurization systems. Environmental Science and Pollution Research. 28(34), 46089–46099. DOI: https://doi.org/10.1007/s11356-020-11500-w

[11] Chen, J., 2022. Changing Patterns of the Flow Ratio with the Distance of Exhaust and Supply Hood in a Parallel Square Push-Pull Ventilation. International Journal of Environmental Research and Public Health. 19(5), 2957. DOI: https://doi.org/10.3390/ijerph19052957

[12] Logachev, K.I., Ziganshin, A.M., Averkova, O.A.,

2020. A study of separated flows at inlets of flanged slotted hoods. Journal of Building Engineering. 29, 101159. DOI: https://doi.org/10.1016/j.jobe.2019.101159

[13] Methner, M.M., 2010. Effectiveness of a Custom-fitted Flange and Local Exhaust Ventilation (LEV) System in Controlling the Release of Nanoscale Metal Oxide Particulates During Reactor Cleanout Operations. International Journal of Occupational and Environmental Health. 16(4), 475–487.

[14] Zhang, W., Guo, C.M., Zhang, Z.G., et al., 2006. Numerical simulation of airflow pattern in gas-collecting hood of aerated grit chamber. Journal of Tianjin Chengjian University. 2006(1), 31–34. (in Chinese)

[15] Guo, J.Z., Bao, J.L., 2008. Gas Flow-Field Numerical Simulation and Capture Effect of Up-suction Hood. Journal of Environment and Health. 25(9), 786–788. (in Chinese)

[16] Liu, Q.H., 2014. The flow field characteristics of one-side constrained buoyant jet and optimization research of exhaust hood [Master's Thesis]. Xi'an University of Architecture & Technology: Xi'an, China. (in Chinese)

[17] Song, G.J., Yang, L., Shen, H.G., 2011. A CFD study on optimal venting volume and air flow distribution in a special designed hood system for controlling dust flow. China Foundry. 8(3), 316–320.

[18] Zhang, Q., Wang, Y., Zhang, W., et al., 2019. Energy and resource conservation and air pollution abatement in China's iron and steel industry. Resources, Conservation and Recycling. 147, 67–84. DOI: https://doi.org/10.1016/j.resconrec.2019.04.018

[19] Ren, G.X., Wang, Y., 2010. Study on capture efficiency of local exhaust hood for high-temperature dust source. Journal of Guangzhou University. 9(3), 76–79. (in Chinese)

[20] Wang, Y., Meng, X., Yang, X., et al., 2014. Influence of convection and radiation on the thermal environment in an industrial building with buoyancy-driven natural ventilation. Energy and Buildings. 75, 394–401. DOI: https://doi.org/10.1016/j.enbuild.2014.02.031

[21] Huai, W., Li, Z., Qian, Z., et al., 2010. Numerical Simulation of Horizontal Buoyant Wall Jet. Journal of Hydrodynamics. 22(1), 58–65. DOI: https://doi.org/10.1016/S1001-6058(09)60028-7

[22] Naffouti, T., Zinoubi, J., Maad, R.B., 2010. Experimental characterization of a free thermal plume and in interaction with its material environment. Applied Thermal Engineering. 30(13), 1632–1643. DOI: https://doi.org/10.1016/j.applthermaleng.2010.03.021

[23] Zukowska, D., Melikov, A., Popiolek, Z., 2012. Impact of personal factors and furniture arrangement on the thermal plume above a sitting occupant. Building and Environment. 49, 104–116. DOI: https://doi.org/10.1016/j.buildenv.2011.09.015

[24] Zhang, J., Lou, C., Xie, M., et al., 2025. Ventilation performance evaluation of rectangular jet-enhanced exhaust hood under the influence of thermal contamination jet in industrial buildings. Case Studies in Thermal Engineering. 68, 105948. DOI: https://doi.org/10.1016/j.csite.2025.105948

[25] Sun, H., Feng, Q., Long, J., et al., 2025. Study on the control effect of exhaust hood on entrained air during particles flow falling and wall collision process. Granular Matter. 27(1), 22. DOI: https://doi.org/10.1007/s10035-024-01501-8

[26] Liu, Y., Bao, L., Wang, H., et al., 2023. Reduced-scale experimental investigation on flow field characteristics of exhaust hood of double helix lifting transportation equipment in an industrial plant. Case Studies in Thermal Engineering. 43, 102798. DOI: https://doi.org/10.1016/j.csite.2023.102798